

Article

Experimental Demonstration to Enhance the Curvature Sensitivity of a Fiber Mach–Zehnder Interferometer Based on a Waist-Enlarged Technique Using Polymer

Laura G. Martínez-Ramírez ¹, Iván Hernández-Romano ^{2,*}, Cipriano Guzmán-Cano ¹,
Sigifredo Marrujo-García ¹, Arturo A. Fernández-Jaramillo ³, Julian M. Estudillo-Ayala ¹,
Roberto Rojas-Laguna ¹ and Juan M. Sierra-Hernández ¹

¹ Electronics Department, DICIS, University of Guanajuato, Salamanca 36885, Mexico; lg.martinezramirez@ugto.mx (L.G.M.-R.); mc.guzmancano@ugto.mx (C.G.-C.); s.marrujogarcia@ugto.mx (S.M.-G.); julian@ugto.mx (J.M.E.-A.); rlaguna@ugto.mx (R.R.-L.); jm.sierrahernandez@ugto.mx (J.M.S.-H.)

² CONAHCYT-Electronics Department, University of Guanajuato, Salamanca 36885, Mexico

³ Unidad Académica de Ingeniería Biomédica, Universidad Politécnica de Sinaloa, Carretera Municipal Libre Mazatlán Higuera Km 3, Col. Genaro Estrada, Mazatlán 82199, Mexico; aferandez@upsin.edu.mx

* Correspondence: hromano@ugto.mx

Abstract: A fiber curvature sensor based on a Mach–Zehnder Interferometer (MZI) constructed using the waist-enlarged technique to splice a segment of non-zero dispersion-shifted fiber (NZ-DSF) between two segments of single mode fiber (SMF) is proposed and experimentally demonstrated. All fabricated sensors presented an improvement in their curvature sensitivity when they were coated with polydimethylsiloxane (PDMS) polymer. The sensor that exhibited the best performance was 6.5 cm long, with a curvature sensitivity of 8.27 nm/m⁻¹ in a range of 0.69 m⁻¹ (from 1.08 to 1.77 m⁻¹). This sensitivity is 3.22 times higher than that of the sensor without polymer. Additionally, the sensor coated with polymer exhibited cross-sensitivity that is 2.23 times smaller than the sensor without polymer. The easy fabrication and notable performance of this device makes it alluring for structural health monitoring.

Keywords: waist-enlarged; PDMS polymer; non-zero dispersion-shifted fiber; curvature sensor



Citation: Martínez-Ramírez, L.G.; Hernández-Romano, I.; Guzmán-Cano, C.; Marrujo-García, S.; Fernández-Jaramillo, A.A.; Estudillo-Ayala, J.M.; Rojas-Laguna, R.; Sierra-Hernández, J.M.

Experimental Demonstration to Enhance the Curvature Sensitivity of a Fiber Mach–Zehnder Interferometer Based on a Waist-Enlarged Technique Using Polymer. *Photonics* **2024**, *11*, 262. <https://doi.org/10.3390/photonics11030262>

Received: 3 February 2024

Revised: 2 March 2024

Accepted: 11 March 2024

Published: 14 March 2024



Copyright: © 2024 by the authors. Licensee MDPI, Basel, Switzerland. This article is an open access article distributed under the terms and conditions of the Creative Commons Attribution (CC BY) license (<https://creativecommons.org/licenses/by/4.0/>).

1. Introduction

Monitoring curvature is vital for innumerable applications, such as reconstructing 2D circle-shaped objects using curvature radius sensing [1], trailing deformation in aircraft [2], and monitoring vital signs [3]. Consequently, fiber optic curvature sensors have been widely researched by academic groups and industries worldwide. Several fiber optics sensors have been fabricated using specialty optical fibers such as suspended-core fiber (SCF) [4], dispersion compensation fiber (DCF) [5], seven-core fiber (SCF) [6], C-fiber [7], hollow core fiber (HCF) [8], negative curvature hollow core fiber (NCHCF) [9], and ring core few-mode fiber (RC-FMF) [10]. Not only are specialty fibers used to construct curvature sensors, but SMF is also used. Accomplishing this purpose requires that the fiber structure be modified using special techniques. For instance, femtosecond lasers can be used to inscribe a waveguide in the fiber core [11] or a cladding waveguide can be used to construct an MZI [12]. Another technique is to polish the lateral side of an SMF to obtain a D-shaped optical fiber curvature sensor [3]. On the other hand, the use of PDMS polymer in the process of the fabrication of fiber sensors has attracted attention due to its low cost, as well as the simple way of preparing and curing it. It has been used to facilitate packaging for applications that require rough handling [13], as well as enhance their curvature sensitivity [14]. Moreover, it has been shown that a microfiber and a microfiber knot embedded in PDMS can be used to measure pressure [15] and longitudinal strain [16], respectively.

Here, we proposed a fiber curvature sensor based on a waist-enlarged technique. The sensor was fabricated using a segment of NZ-DSF between two segments of SMF. The waist of the splices is enlarged, and they are manufactured by using a conventional machine splicer, where the waist-enlarged splices behave like mode couplers and the segment of NZ-DSF is the sensing part of the device; the whole fiber structure works like an MZI. It is worth mentioning that this fiber has a central core, and a ring core surrounds it. It has been shown that fibers that have ring cores are sensitive to curvature perturbation [17]. Different lengths of NZ-DSF were tested, and we found experimentally that the 5 cm long sample showed the highest curvature sensitivity (-4.86 nm/m^{-1} from 1.25 to 1.77 m^{-1}). To make the sensors sturdier and more sensitive, they were packaged with PDMS polymer, and curvature sensitivity increased in all cases. An additional benefit of this covering polymer is the low temperature cross-sensitivity. In the end, we observed that the sensor that exhibited the better performance was 6.5 cm long, with a curvature sensitivity of 8.27 nm/m^{-1} in a range of 0.69 m^{-1} (from 1.08 to 1.77 m^{-1}).

2. Fabrication Process and Operation Principle

The MZIs were fabricated using a segment of NZ-DSF (DCF4, Thorlabs, NJ, USA) between two segments of SMF; its core, ring core, and cladding diameters were 5.8, 16, and $125 \mu\text{m}$ [18], respectively. The splices were achieved by employing a conventional electrical discharge splicer (model S175, Fitel, Tokyo, Japan) operated in manual mode; the discharge parameters that were used can be summarized as follows: pre-fusion time of 210 ms, arch power of 119 mW, and overlap set at $50 \mu\text{m}$. In the following description of the fabrication process, the waist-enlarged splices were accomplished using these parameters. In order to realize better control of the length of the MZI, a precise cutting system was implemented. This experimental setup was assembled using a linear translation stage with an integrated controller (LTS150, Thorlabs, NJ, USA), a laptop, magnets, and a fiber cleaver. The fabrication process of these MZIs is described in the following steps. First, it is necessary to strip off the coating of the tip of the SMF and the whole segment of the NZ-DSF to accomplish the first splice. A segment of SMF is then fixed with two magnets in the linear translation stage, and the rest of the segment of fiber is on the fiber cleaver. After cleaving the SMF, the segments of SMF and NZ-DSF are placed in the splicer holders, and their position is adjusted to align their cores and thus perform the splice discharge, as can be seen in Figure 1a,b.

Afterward, with the right motor, an overlap of $50 \mu\text{m}$ is achieved and another discharge is applied (see Figure 1c). The previous step is carried out 25 times, forming the waist-enlarged splice, as shown in Figure 1d. Consequently, the waist-enlarged splice is taken from the splicer and is set on the cleaver. The linear translation stage then moves to a specific length and an accurate segment (five different lengths from 5 to 7 cm, in steps of 0.5 cm) of the NZ-DSF is cut with the cleaver. For the second part of the sensor, the steps of the first splice are repeated (see Figure 1e–h). Finally, the full sensor is realized, as shown in Figure 1i. A lateral view of one of the fabricated devices is shown in Figure 2; it is easy to observe that the waist enlargement technique increases the diameter of both splices; it is essential to mention that both waist-enlarged splices work as a mode coupler. The diameters of the lead-in and the lead-out waist-enlarged splices are $307 \mu\text{m}$ and $308 \mu\text{m}$, respectively, as shown in Figure 2. All the sensors used in this experiment have a waist-enlarged splice diameter in the range of $15 \mu\text{m}$, from 300 to $315 \mu\text{m}$, since fulfilling this condition generates better fringe contrast.

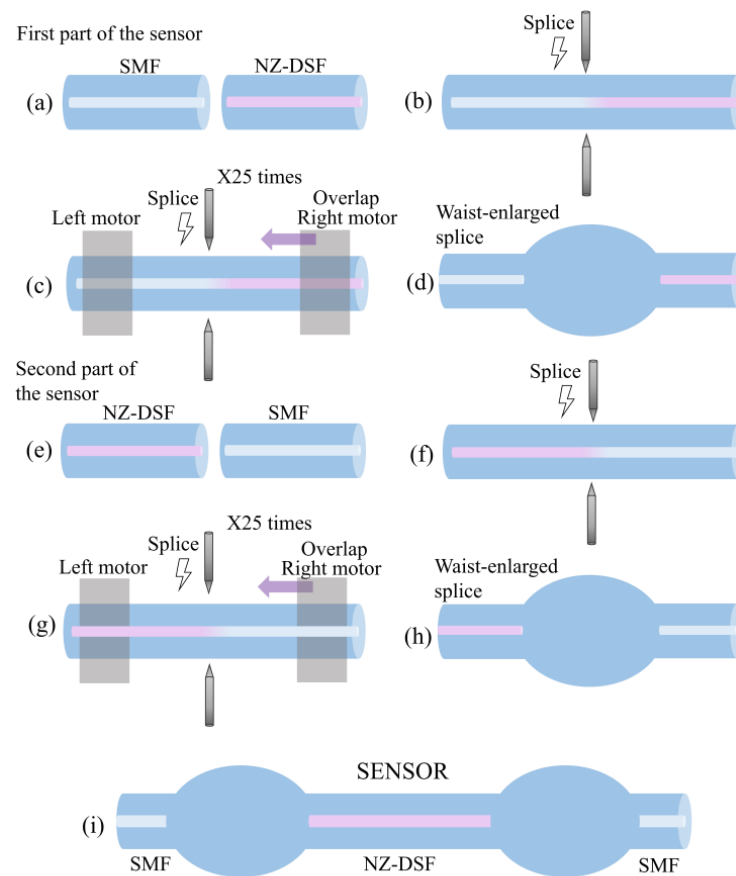


Figure 1. Fabrication process of the MZI. (a) SMF and NZ-DSF segments placed on the splicer (b) Splicing SMF and NZ-DSF, (c) Overlap the right motor, (d) Lead-in waist-enlarged splice, (e) NZ-DSF and SMF segments placed on the splicer, (f) Splicing NZ-DSF and SMF, (g) Overlap the right motor, (h) Lead-out waist-enlarged splice, (i) Drawing of the sensor.

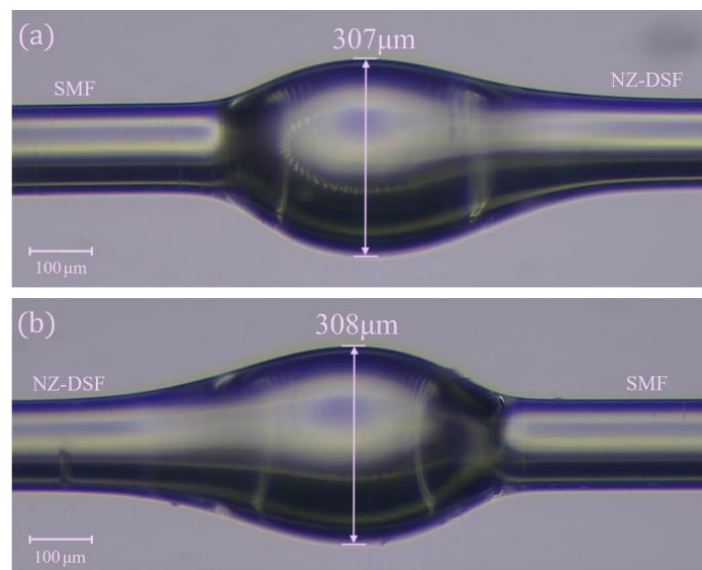


Figure 2. A microscope image of (a) the lead-in waist-enlarged splice and (b) the lead-out waist-enlarged splice.

The next step is to cover the sensor with a polymer, since this process has been demonstrated to increase curvature sensitivity [14]. Thus, the coating process began by placing each sensor on a flexible steel sheet, in which three layers of adhesive tape were cut and placed at the ends to obtain a height of 1 mm. The sensor was set above the tape layers to prevent contact between the sensing area and the steel sheet. After the sensor was centered and fixed, it was coated with the polymer following the manufacturer’s specifications. Additionally, other advantages of packaging this device include avoiding contamination of the sensing area with dust or other substances and increasing the resistance of the sensor to perform heavy-duty work. To analyze the output signal of each MZI (different lengths) without and with polymer, an experimental setup was implemented (see Figure 3). The Superluminescent Diode (SLD-1550S-A40, Thorlabs, Newton, NJ, USA) was used as a broadband source and a polarization controller was added to adjust the polarization state, which helps to obtain higher fringe visibility. The output spectra of the sensors were measured with an Optical Spectrum Analyzer (OSA) (MS9740B, Anritsu, Atsugi-shi, Kanagawa, Japan).

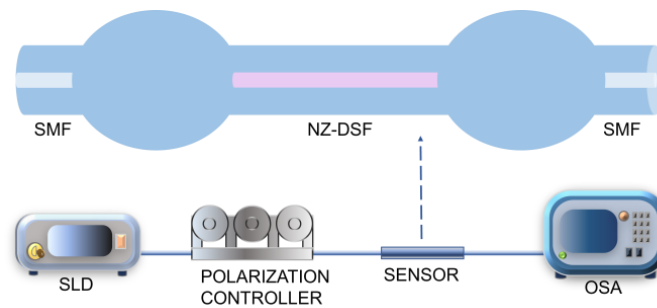


Figure 3. Experimental setup to test the transmission of MZIs.

The experimental spectra of the different MZIs are shown in Figure 4a. At 1550 nm, it is observed that the maximum value of the Free Spectral Range (FSR) is 10.44, 12.44, 8.88, 7.72, and 6.76 nm for the sensors of 5, 5.5, 6, 6.5, and 7 cm in length, respectively. The maximum value of the fringe contrast at 1550 nm is 17.7, 28, 27.7, 13.4, and 21.4 dB for the sensors of 5, 5.5, 6, 6.5, and 7 cm in length, respectively. Figure 4b shows the FFT of the different spectra; they present several peaks, which means that more than two modes are propagating in the sensor and that they are interfering.

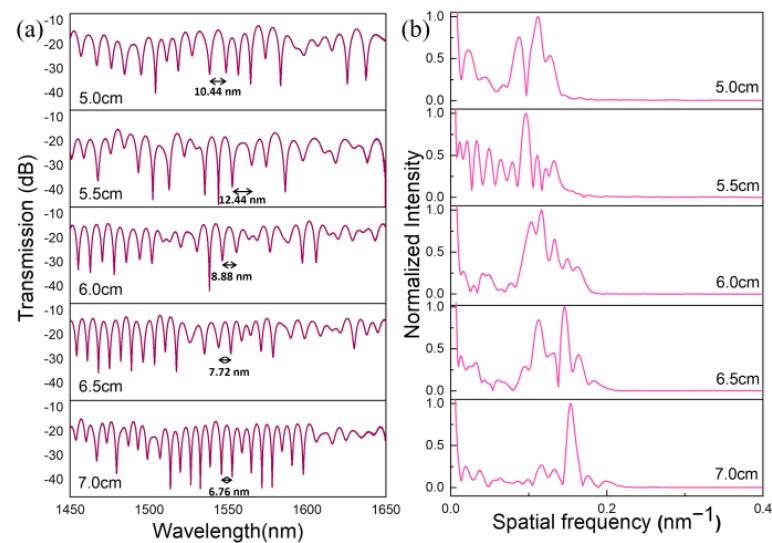


Figure 4. (a) The transmission spectra of different lengths of MZI. (b) FFT of the transmission spectra.

The experimental spectra of the different MZIs coated with polymer are shown in Figure 5a. This figure shows that the maximum MZI values at 1550 nm in terms of the *FSR* are 11, 7.96, 7.72, 8.24, and 7.16 nm for the sensors of 5, 5.5, 6, 6.5, and 7 cm in length, respectively. The maximum values of the fringe contrast at 1550 nm are 24.5, 23.9, 28.5, 17.2, and 13.7 dB for the sensors of 5, 5.5, 6, 6.5, and 7 cm in length, respectively. Figure 5b shows the FFT of the different spectra; the presence of various peaks can be explained as in the previous case.

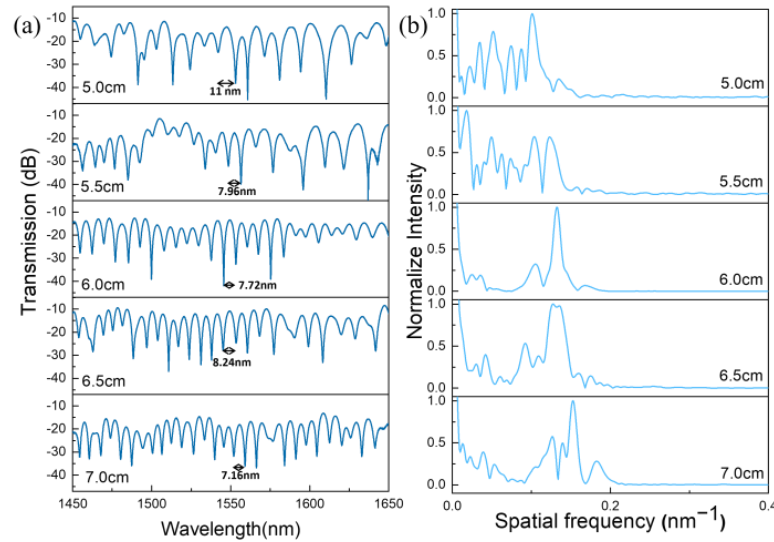


Figure 5. MZIs of different lengths covered with polymer: (a) the transmission spectra, (b) the FFT of the transmission spectra.

Comparing the performance of the devices using the spectra at 1550 nm, we observe that the MZIs with a length of 5, 6.5, and 7 cm increment their *FSR* when they are covered with the polymer, and the MZIs with a length of 5, 6, and 6.5 cm augment their contrast when they are coated with the polymer. In the other cases, the *FSR* and contrast decrease. Regarding the FFT of the MZIs, it is easy to notice that the MZI with a length of 6 cm when covered with polymer has fewer peaks than the same device without polymer. This means that the number of modes that interfere decreases. In the other cases, we observe various peaks presented in the FFT, which means that several modes travel in the sensor with or without polymer.

The principle of operation of the MZI can be explained as follows: The waist-enlarged splices between the SMF and NZ-DSF act as optical couplers. This allows for the launch of light to the core, ring, and cladding in the NZ-DSF central segment. These modes travel in the section of the NZ-DSF until they are recombined in the output waist-enlarged splice, producing an interference pattern at the sensor output. As was mentioned in the previous paragraph, the *FSR* of the output spectra was changed after they were coated with a polymer. Due to this, we believe the interference pattern strongly depends on the (Effective Refractive Index) ERI of the cladding modes. It is important to note that the ERI values of these modes are the only ones modified when the (Refractive Index) RI of the surrender changes. Moreover, by observing the FFT of the signal, we observe that the core mode is also present and that the ring modes could be presented, though they do not significantly modify the *FSR* of the interference pattern. Assuming all these facts, we can express the interference pattern using the following equation [19]:

$$I = I_{core} + \sum_m I_{clad}^m + \sum_m 2(I_{core} I_{clad}^m)^{1/2} \cos \Phi^m \quad (1)$$

where I , I_{core} , and I_{clad}^m are the intensity of the interference pattern, the intensity of the core, and intensity of the m th cladding mode, respectively, and Φ^m is the phase. The phase can be expressed in terms of the ERI of the core mode and cladding modes as follows [19]:

$$\Phi^m = \frac{4\pi(n_{eff}^{core} - n_{eff}^{clad,m})L}{\lambda_m} = \frac{4\pi\Delta n_{eff}^m L}{\lambda_m} \tag{2}$$

where n_{eff}^{core} and $n_{eff}^{clad,m}$ are the ERI values of the core mode and cladding modes, L is the length of the NZ-DSF, λ_m is the wavelength of light in a vacuum, and Δn_{eff}^m is the ERI difference. It should be noted that the FSR of the interference pattern can be expressed by $FSR = \lambda^2 / \Delta n_{eff}^m L$.

For simplicity, we analyzed two possible cases when the sensor is curved: (i) The sensor is not covered with polymer. Under these conditions, the fiber undergoes strain, causing a change in n_{eff}^{core} and $n_{eff}^{clad,m}$ (due to photoelastic coefficient [20,21]) and producing phase displacement of the transmission dip. (ii) The sensor is covered with polymer. As in the previous case, the n_{eff}^{core} and $n_{eff}^{clad,m}$ values are modified due to the curvature. Furthermore, the polymer around the fiber is strained, which generates an RI change in the polymer. This causes a change in the value of $n_{eff}^{clad,m}$, which is observable when the polymer is present (this property is otherwise (air) not exhibited (photoelastic coefficient)). Therefore, using the polymer, $n_{eff}^{clad,m}$ is modified by the photoelastic effect of the fiber and the polymer; both contributions increase the curvature sensitivity of the sensor, as will be shown in the experimental section.

3. Experimental Results

3.1. Experimental Setup for Performing Curvature Measurements

The following measurements were carried out to determine the different MZIs' curvature properties (the experimental setup is shown in Figure 6). The SLD was used as a broadband source, and a polarization controller was added to adjust the polarization state. The MZI was attached to a flexible steel sheet, and the steel sheet was then set between two mechanical supports, one of which was fixed to a translation stage. This stage had a micrometer that allowed for lateral displacement, producing different curvatures that the steel sheet underwent (as well as the sensor). The output spectra were measured with an OSA. The curvature is obtained as follows [22]:

$$C = \frac{1}{R} \cong \left(\frac{24x}{L_0^3} \right)^{\frac{1}{2}} \tag{3}$$

where R is the radius of the curvature, L_0^3 is the length of the flexible steel sheet, and x is the lateral displacement that modifies the curvature. Five different lengths of MZI were curved within the range of 0 to 1.77 m⁻¹.

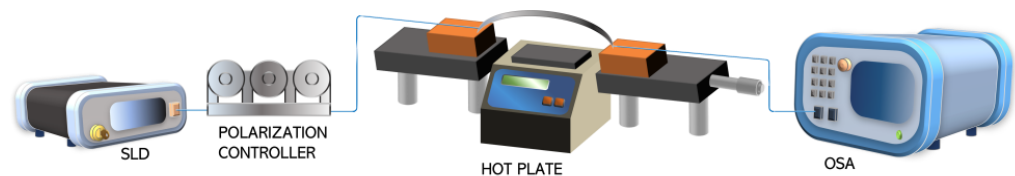


Figure 6. Experimental setup for curvature measurements.

It has been found that the phase of the MZI spectrum changes according to the curvature that the sensor observes; this behavior was exhibited by all sensors presented here. Three parameters that are essential to know to get a better insight into the performance of this kind of sensor are curvature sensitivity (with its associated error), curvature range,

and R-square values. The sensors without polymer coatings were characterized using the setup shown in Figure 6, and the related vital information is shown in Table 1. The measurements were carried out three times and the mean value was then calculated, with the standard deviation finally obtained to estimate the associated error.

Table 1. Curvature of MZIs without polymer.

L (cm)	Curvature Sensitivity (nm/m ⁻¹)	Curvature Range (m ⁻¹)	R-Square
5	-4.86 ± 0.35	From 1.25 to 1.77 (0.52)	0.98
5.5	-3.28 ± 0.16	From 1.08 to 1.53 (0.45)	0.99
6	-2.50 ± 0.14	From 0.88 to 1.53 (0.65)	0.98
6.5	-2.57 ± 0.15	From 1.08 to 1.77 (0.69)	0.98
7	-4.46 ± 0.44	From 0.62 to 1.39 (0.77)	0.97

The MZI with a length of 5 cm presented the highest curvature sensitivity (-4.86 ± 0.35 nm/m⁻¹) and a curvature range from 1.25 to 1.77 m⁻¹ (0.52 m⁻¹). Furthermore, the MZI with a length of 7 cm obtained the highest curvature range, from 0.62 to 1.39 m⁻¹ (0.77 m⁻¹), and a curvature sensitivity of -4.46 ± 0.44 nm/m⁻¹. After this characterization, all the MZIs were coated with the polymer described in Section 2. As the polymer attached the sensor to the steel sheet, curvature measurements were achieved using the setup of Figure 6, and Table 2 shows their results. The MZI with a length of 6.5 cm exhibited better performance: its curvature sensitivity and curvature range were 8.27 ± 0.76 nm/m⁻¹ and 0.69 m⁻¹ (from 1.08 to 1.77 m⁻¹), respectively. This sensor showed the best upgrade, specifically an increase in sensitivity by 3.22 times and a 119% augmentation in curvature range. The following paragraphs will show only the experimental results (curvature and temperature response) of this sensor (6.5 cm long) without and with polymer.

Table 2. Curvature of MZIs with polymer.

L (cm)	Curvature Sensitivity (nm/m ⁻¹)	Curvature Range (m ⁻¹)	R-Square
5	-6.44 ± 0.52	From 0.88 to 1.39 (0.51)	0.98
5.5	-7.26 ± 1.11	From 1.25 to 1.77 (0.52)	0.93
6	-7.40 ± 1.27	From 0.88 to 1.39 (0.51)	0.94
6.5	8.27 ± 0.76	From 1.08 to 1.77 (0.69)	0.95
7	7.13 ± 1.98	From 0.88 to 1.39 (0.51)	0.86

To compare the performance of the MZI with a length of 6.5 cm as a curvature sensor both without and with polymer, one can observe that the transmission spectra of the sensor without polymer underwent a blueshift as the curvature increased. Figure 7a exhibits the dip that presents the higher wavelength displacement as the curvature increases. We observed a linear response between curvature and wavelength displacement for curvatures from 1.08 to 1.77 m⁻¹ (0.69 m⁻¹) with curvature sensitivity of -2.57 ± 0.15 nm/m⁻¹, as shown in Figure 7b. It is worth mentioning that the micrometer that was used for this experiment allows lateral displacement of 0.5 mm, producing different curvatures. The maximum lateral displacement of the micrometer was 4 mm, and this value corresponds to a curvature of 1.7693 m⁻¹.

The sensor when coated with polymer exhibits a curvature sensitivity of 8.27 ± 0.76 nm/m⁻¹ in the range of 1.08 to 1.77 m⁻¹ (0.69 m⁻¹), as shown in Figure 8a,b. It has been found that coating the MZI with polymer increased sensitivity by three times.

3.2. Temperature Measurement without and with Polymer

The experimental setup shown in Figure 6 was used to obtain temperature response values. At zero curvature, the sensor was set on a hotplate at different temperatures from

20 to 80 °C in steps of 15 °C. Figure 9a shows the redshift of one dip of the spectral response, and its temperature sensitivity was 0.049 ± 0.002 nm/°C, as shown in Figure 9b.

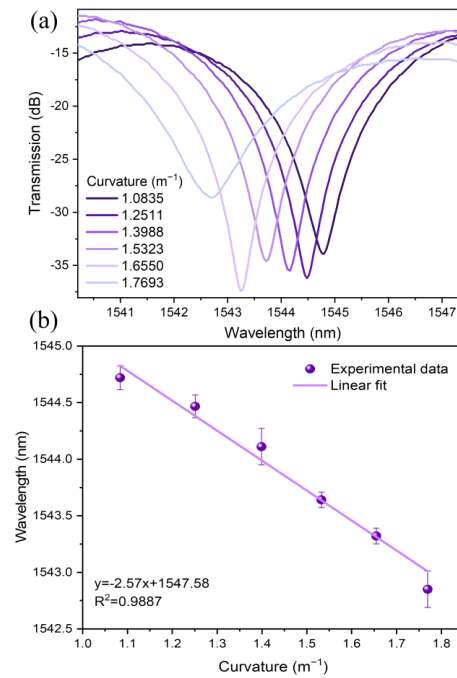


Figure 7. (a) The spectral response at different curvatures for the 6.5 cm long sensor. (b) The linear relationship between the curvature and wavelength for the 6.5 cm long sensor.

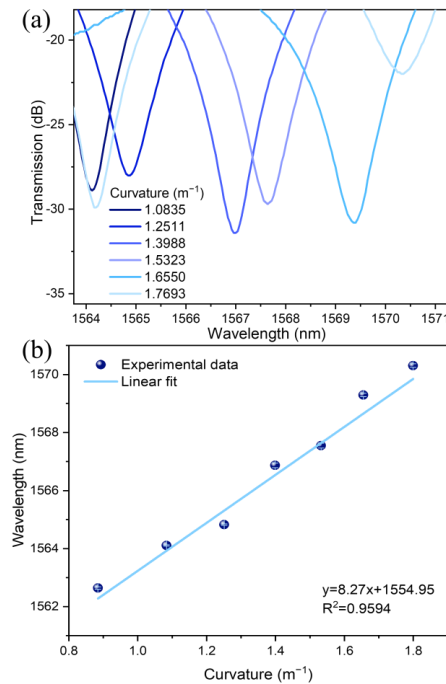


Figure 8. (a) The spectral response at different curvatures for the 6.5 cm long sensor coated with the polymer. (b) The linear relationship between the curvature and wavelength for the 6.5 cm long sensor coated with the polymer.

The same characterization was carried out for the sensor coated with polymer. Figure 10a shows the spectral response at different temperatures, and its temperature sensitivity was 0.071 ± 0.0009 nm/°C, as shown in Figure 10b. From this figure, it can be seen that tempera-

ture sensitivity increased by 1.44 times compared to the sensitivity of the sensor without polymer.

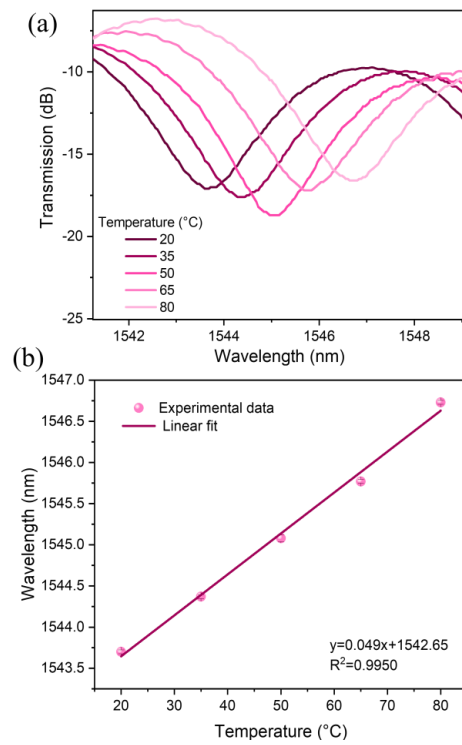


Figure 9. (a) The spectral response at different temperatures for the 6.5 cm long sensor. (b) The linear relationship between the temperatures and wavelength for the 6.5 cm long sensor.

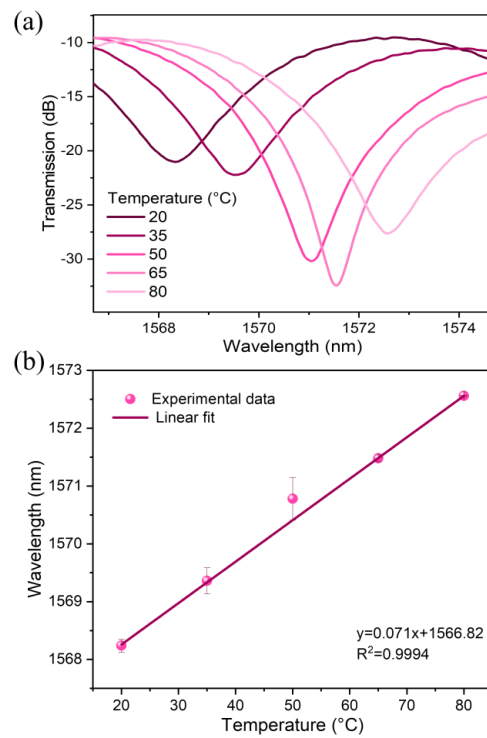


Figure 10. (a) The spectra response at different temperatures for the 6.5 cm long sensor coated with the polymer. (b) The linear relationship between the temperatures and wavelength for the 6.5 cm long sensor coated with the polymer.

4. Results and Discussion

It is important to analyze the performance of the sensor when not covered with polymer. Its curvature and temperature sensitivities were -2.57 nm/m^{-1} and $0.049 \text{ nm/}^\circ\text{C}$, respectively. Cross-sensitivity was $0.019 \text{ m}^{-1}/^\circ\text{C}$, and this low value allows us to neglect temperature during curvature measurements. On the other hand, the sensor coated with polymer exhibited curvature and temperature sensitivities of 8.27 nm/m^{-1} and $0.071 \text{ nm/}^\circ\text{C}$, respectively. Cross-sensitivity was $0.0085 \text{ m}^{-1}/^\circ\text{C}$, which is 2.23 times smaller than the sensor without polymer. This means that during curvature measurements, the temperature changes do not affect the curvature value of the polymer-coated sensor as much as they do for the sensor without polymer, making the sensor coated with polymer more suitable for real applications. Another essential parameter that should be considered when we analyze the performance of a sensor is the Q-factor, which offers information regarding sensitivity, resolution, and accuracy [23]. We calculated the Q-factor considering a 3 dB bandwidth and the central wavelength of the dip [24]. From Table 3, we observed, for curvature measurements, that the dips of the sensor without polymer had a higher Q-factor than the dips of the sensor with polymer (except for the curvature of 1.7693 m^{-1}). On the contrary, for temperature measurement, the dips of the sensor without polymer had a lower Q-factor than the dips of the sensor with polymer within the range of 35 to $80 \text{ }^\circ\text{C}$ (see Table 4). The dips having a higher Q-factor means that they will exhibit lower spectral transmission noise, implying an upgrade in the performance of the sensor [25].

Table 3. The Q-factor values of the dips corresponding to different curvatures.

Curvature (m^{-1})	Curvature without Polymer		Curvature with Polymer	
	The Central Wavelength of the Dip (nm)	Q-Factor	The Central wavelength of the Dip (nm)	Q-Factor
1.0835	1544.76	3960.92	1564.12	3066.90
1.2511	1544.48	5148.27	1564.84	2301.24
1.3988	1544.16	4981.16	1566.96	2901.78
1.5323	1543.72	4540.35	1567.64	2449.44
1.655	1543.24	5511.57	1569.36	2414.40
1.7693	1542.68	1623.87	1570.36	1308.63

Table 4. The Q-factor values of the dips corresponding to different temperatures.

Temperature ($^\circ\text{C}$)	Temperature without Polymer		Temperature with Polymer	
	The Central Wavelength of the Dip (nm)	Q-Factor	The Central Wavelength of the Dip (nm)	Q-Factor
20	1543.7	799.84	1568.36	780.28
35	1544.37	808.57	1569.52	1171.28
50	1545.08	908.87	1571.04	2182.00
65	1545.77	796.79	1571.56	2965.21
80	1546.73	761.94	1572.56	1512.08

The Detection Limit (DL) needs to be evaluated in order to acquire a better understanding of the performance of a device. The equation that is used to calculate this value is $DL = R/S$ [25], where R and S are the wavelength scanning resolution of the OSA and the sensitivity of the sensor, respectively. The resolution used to obtain the curvature measurement was 0.07 nm ; thus, the DL values for the sensor without and with polymer were 0.0272 and 0.0085 m^{-1} , respectively. The maximum wavelength scanning resolution of the OSA is 0.03 nm . Using this resolution, it is possible to achieve a DL of 0.0117 m^{-1} for the sensor without polymer and 0.0036 m^{-1} for the sensor with polymer. In both cases, the sensor with polymer has a smaller DL due to its higher curvature sensitivity. This means that the sensor with polymer is able to measure smaller curvature changes accurately.

Comparing the performance of our sensor with other fiber optic sensors is an important issue that lets us understand the reliability of our device. Table 5 lists sensors with different fiber structures along with their curvature sensitivities and curvature ranges. Sensors 2, 3, 5, and 6 reported lower curvature sensitivity than our sensor. Sensors 1 and 4 offered the highest curvature sensitivity. However, sensor 1 consisted of two cascading abrupt tapers in an SMF; to manufacture the sensor, they used a CO₂ laser, which makes the fabrication process expensive. Sensor 4 was fabricated using a lateral offset splice of SMF between a four-core fiber (FCF), which, considering the orientation of the special fiber, increases the complexity of the process and is additionally more costly. As a result, our proposed sensor coated with polymer shows competitive curvature sensitivity and an easy fabrication process without costly material that packages the device for potential application in structural health monitoring.

Table 5. Different sensors.

[#]	Structure	Sensitivity (nm/m ⁻¹)	Curvature Range (m ⁻¹)	Reference
1	SMF cascading abrupt tapers	−25.946	From 6.38 to 7.98 (1.6)	[26]
2	MCO-LPFG	0.1877	From 1.775 to 3.436 (1.661)	[27]
3	LPGs in MCF	−4.85	From 0 to 1.77 (1.77)	[28]
4	SMF-FCF-SMF with lateral offset	−18.75	From 0.042 to 0.163 (0.121)	[29]
5	SMF-NCF-RCF-SMF	−3.68	From 1.3856 to 3.6661 (2.28)	[30]
6	SMF-MMF-PCF-MMF-SMF	−1.03	From 10 to 22.4 (12.4)	[31]
7	Our sensor (SMF-NZDSF-SMF)	8.27	From 1.08 to 1.77 (0.69)	---

5. Conclusions

In summary, we have proposed and experimentally demonstrated a fiber curvature sensor based on an MZI that was constructed using the waist-enlarged technique to splice a segment of NZ-DSF between two segments of SMF. Different lengths of NZ-DSF were tested, and the 5 cm long sample showed the highest curvature sensitivity (−4.86 nm/m⁻¹, from 1.25 to 1.77 m⁻¹). All these sensors were packaged using PDMS polymer to exploit the advantages of this technique, such as augmented mechanical strength, protection against dust, and increased sensitivity. We experimentally demonstrated that the curvature sensitivity of all the sensors coated with polymer increases; the device with a length of 6.5 cm presented the highest curvature sensitivity (8.27 nm/m⁻¹, from 1.08 to 1.77 m⁻¹). Additionally, the sensor coated with polymer exhibited cross-sensitivity that was 2.23 times smaller than the sensor without polymer. All of these remarkable features, as well as the accessible and highly reproducible fabrication process, lead us to believe that this device has potential application in structural health monitoring.

Author Contributions: Conceptualization, L.G.M.-R., I.H.-R. and J.M.S.-H.; methodology, L.G.M.-R., I.H.-R. and J.M.S.-H.; validation, L.G.M.-R., I.H.-R., C.G.-C., S.M.-G., A.A.F.-J., J.M.E.-A., R.R.-L. and J.M.S.-H.; formal analysis, L.G.M.-R., I.H.-R., C.G.-C., S.M.-G. and J.M.S.-H.; investigation, L.G.M.-R., I.H.-R. and J.M.S.-H.; resources, I.H.-R., A.A.F.-J., J.M.E.-A. and R.R.-L.; software, L.G.M.-R., C.G.-C. and S.M.-G.; data curation, L.G.M.-R., I.H.-R., C.G.-C. and S.M.-G.; writing—original draft preparation, L.G.M.-R. and I.H.-R.; writing—review and editing, L.G.M.-R., I.H.-R., C.G.-C., S.M.-G., A.A.F.-J., J.M.E.-A., R.R.-L. and J.M.S.-H.; visualization, L.G.M.-R., I.H.-R., C.G.-C., S.M.-G., A.A.F.-J., J.M.E.-A., R.R.-L. and J.M.S.-H.; supervision, I.H.-R. and J.M.S.-H.; project administration, I.H.-R., A.A.F.-J.,

J.M.E.-A. and R.R.-L.; funding acquisition, I.H.-R. and J.M.S.-H. All authors have read and agreed to the published version of the manuscript.

Funding: This work was supported by Universidad de Guanajuato under Grant CIIC-105/2023.

Institutional Review Board Statement: Not applicable.

Informed Consent Statement: Not applicable.

Data Availability Statement: Data are contained within the article.

Acknowledgments: Laura G. Martinez-Ramirez is grateful to CONAHCyT for a Ph.D. scholarship (No. 893844), and Guzmán-Cano is also grateful to CONAHCyT for a Ph.D. scholarship. I. Hernández Romano gratefully acknowledges the generous financial support of Universidad de Guanajuato.

Conflicts of Interest: The authors declare no conflicts of interest. The funders had no role in the design of the study; in the collection, analyses, or interpretation of data; in the writing of the manuscript; or in the decision to publish the results.

References

- Chen, Z.; Wang, C.; Ding, Z.; Zhu, D.; Guo, H.; Pan, M.; Yu, Y.; Liu, K.; Jiang, J.; Liu, T. Demonstration of Large Curvature Radius Shape Sensing Using Optical Frequency Domain Reflectometry in Multi-Core Fibers. *IEEE Photonics J.* **2021**, *13*, 1–9. [[CrossRef](#)]
- Arrizabalaga, O.; Sun, Q.; Beresna, M.; Lee, T.; Zubia, J.; Velasco Pascual, J.; Sáez De Ocariz, I.; Schülzgen, A.; Antonio-Lopez, J.E.; Amezcua-Correa, R.; et al. High-Performance Vector Bending and Orientation Distinguishing Curvature Sensor Based on Asymmetric Coupled Multi-Core Fibre. *Sci. Rep.* **2020**, *10*, 14058. [[CrossRef](#)] [[PubMed](#)]
- Li, J.; Liu, B.; Liu, J.; Shi, J.-L.; He, X.-D.; Yuan, J.; Wu, Q. Low-Cost Wearable Device Based D-Shaped Single Mode Fiber Curvature Sensor for Vital Signs Monitoring. *Sens. Actuators A Phys.* **2022**, *337*, 113429. [[CrossRef](#)]
- Zhu, F.; Zhang, Y.; Jiang, W.; Qu, Y.; Qi, K.; Guo, Y. Self-Assembled Highly Sensitive Hybrid Structure Sensor for Vector Curvature and Temperature Measurement. *J. Light. Technol.* **2022**, *40*, 2570–2576. [[CrossRef](#)]
- Wang, F.; Zhang, L.; Ma, T.; Wang, X.; Yu, K.; Liu, Y. A High-Sensitivity Sensor Based on Tapered Dispersion Compensation Fiber for Curvature and Temperature Measurement. *Opt. Commun.* **2021**, *481*, 126534. [[CrossRef](#)]
- Ji, Y.; Sun, D.; Chen, Y.; Shi, Y.; Cao, J.; Zhang, G.; Han, Z.; Wang, C.; Zhu, X. A High Sensitivity Curvature Sensor Based on Microfiber Mach-Zehnder Interferometer with Tapered Seven-Core Fiber. *IEEE Sens. J.* **2021**, *21*, 24090–24097. [[CrossRef](#)]
- Sun, Y.; Zhou, X.; Yan, X.; Zhang, X.; Wang, F.; Cheng, T. A Temperature-Insensitive Bidimensional Curvature Sensor Employing C-Fiber-Based Fabry–Pérot Air Cavity. *IEEE Trans. Instrum. Meas.* **2022**, *71*, 1–6. [[CrossRef](#)]
- Li, X.; Liang, J.; Li, J.; Ye, J.; Liu, Y.; Chen, M.; Zhang, Z.; Qu, S. Highly Sensitive Curvature and Temperature Sensor Based on Double Groove Structure and Hollow Core Fiber. *IEEE Sens. J.* **2022**, *22*, 9454–9461. [[CrossRef](#)]
- Yu, Y.; Wang, K.; Zhang, X.; Zhang, Q.; Yang, Y.; Wang, Z.; Huang, Y.; Wen, J.; Chen, W.; et al. High-Sensitive Curvature Sensor Based on Negative Curvature Hollow Core Fiber. *IEEE Sens. J.* **2023**, *23*, 4849–4855. [[CrossRef](#)]
- Zhang, F.; Su, B.; Zhong, L.; Qi, B.; Xu, O.; Qin, Y. Ring Core Few-Mode Fiber Sensor for Curvature Measurement. *Appl. Opt.* **2022**, *61*, 2598. [[CrossRef](#)]
- Rong, Z.; Shu, X.; Xu, Z. Compact Fiber Curvature and Temperature Sensor Inscribed by Femtosecond Laser Through the Coating. *J. Light. Technol.* **2021**, *39*, 3981–3990. [[CrossRef](#)]
- Roldán-Varona, P.; Pallarés-Aldeiturriaga, D.; Rodríguez-Cobo, L.; López-Higuera, J.M. All-in-Fiber Multiscan Mach-Zehnder Interferometer Assisted by Core FBG for Simultaneous Multi-Parameter Sensing. *Opt. Laser Technol.* **2020**, *132*, 106459. [[CrossRef](#)]
- Marrujo-Garcia, S.; Hernandez-Romano, I.; Torres-Cisneros, M.; May-Arrijoja, D.A.; Minkovich, V.P.; Monzon-Hernandez, D. Temperature-Independent Curvature Sensor Based on in-Fiber Mach-Zehnder Interferometer Using Hollow-Core Fiber. *J. Light. Technol.* **2020**, *38*, 4166–4173. [[CrossRef](#)]
- Herrera-Piada, L.A.; Hernández-Romano, I.; May-Arrijoja, D.A.; Minkovich, V.P.; Torres-Cisneros, M. Sensitivity Enhancement of Curvature Fiber Sensor Based on Polymer-Coated Capillary Hollow-Core Fiber. *Sensors* **2020**, *20*, 3763. [[CrossRef](#)]
- Lu, J.; Yu, Y.; Qin, S.; Li, M.; Bian, Q.; Lu, Y.; Hu, X.; Yang, J.; Meng, Z.; Zhang, Z. High-Performance Temperature and Pressure Dual-Parameter Sensor Based on a Polymer-Coated Tapered Optical Fiber. *Opt. Express* **2022**, *30*, 9714. [[CrossRef](#)] [[PubMed](#)]
- Cai, L.; Li, J. PDMS Packaged Microfiber Knot Resonator Used for Sensing Longitudinal Load Change. *J. Phys. Chem. Solids* **2020**, *138*, 109268. [[CrossRef](#)]
- Zhao, W.; Wang, Y.; Li, S.; Geng, W.; Bao, C.; Fang, Y.; Wang, Z.; Liu, Y.; Ren, Y.; Pan, Z.; et al. Non-Zero Dispersion-Shifted Ring Fiber for the Orbital Angular Momentum Mode. *Opt. Express* **2021**, *29*, 25428. [[CrossRef](#)]
- Huerta-Mascotte, E.; Sierra-Hernandez, J.; Mata-Chavez, R.; Jauregui-Vazquez, D.; Castillo-Guzman, A.; Estudillo-Ayala, J.; Guzman-Chavez, A.; Rojas-Laguna, R. A Core-Offset Mach Zehnder Interferometer Based on A Non-Zero Dispersion-Shifted Fiber and Its Torsion Sensing Application. *Sensors* **2016**, *16*, 856. [[CrossRef](#)]
- Rong, Q.; Qiao, X.; Du, Y.; Feng, D.; Wang, R.; Ma, Y.; Sun, H.; Hu, M.; Feng, Z. In-Fiber Quasi-Michelson Interferometer with a Core-Cladding-Mode Fiber End-Face Mirror. *Appl. Opt.* **2013**, *52*, 1441. [[CrossRef](#)]

20. Bertholds, A.; Dandliker, R. Determination of the Individual Strain-Optic Coefficients in Single-Mode Optical Fibres. *J. Light. Technol.* **1988**, *6*, 17–20. [[CrossRef](#)]
21. Albero Blanquer, L.; Marchini, F.; Seitz, J.R.; Daher, N.; Bétermier, F.; Huang, J.; Gervillié, C.; Tarascon, J.-M. Optical Sensors for Operando Stress Monitoring in Lithium-Based Batteries Containing Solid-State or Liquid Electrolytes. *Nat. Commun.* **2022**, *13*, 1153. [[CrossRef](#)] [[PubMed](#)]
22. Gong, H.; Yang, X.; Ni, K.; Zhao, C.-L.; Dong, X. An Optical Fiber Curvature Sensor Based on Two Peanut-Shape Structures Modal Interferometer. *IEEE Photon. Technol. Lett.* **2014**, *26*, 22–24. [[CrossRef](#)]
23. Cai, L.; Zhao, Y.; Li, X. A Fiber Ring Cavity Laser Sensor for Refractive Index and Temperature Measurement with Core-Offset Modal Interferometer as Tunable Filter. *Sens. Actuators B Chem.* **2017**, *242*, 673–678. [[CrossRef](#)]
24. Liu, D.; Wu, Q.; Mei, C.; Yuan, J.; Xin, X.; Mallik, A.K.; Wei, F.; Han, W.; Kumar, R.; Yu, C.; et al. Hollow Core Fiber Based Interferometer for High-Temperature (1000 °C) Measurement. *J. Light. Technol.* **2018**, *36*, 1583–1590. [[CrossRef](#)]
25. White, I.M.; Fan, X. On the Performance Quantification of Resonant Refractive Index Sensors. *Opt. Express* **2008**, *16*, 1020. [[CrossRef](#)] [[PubMed](#)]
26. Niu, L.; Zhao, C.-L.; Gong, H.; Li, Y.; Jin, S. Curvature Sensor Based on Two Cascading Abrupt-Tapers Modal Interferometer in Single Mode Fiber. *Opt. Commun.* **2014**, *333*, 11–15. [[CrossRef](#)]
27. Bai, Z.; Zhang, W.; Gao, S.; Zhang, H.; Wang, L.; Liu, F. Bend-Insensitive Long Period Fiber Grating-Based High Temperature Sensor. *Opt. Fiber Technol.* **2015**, *21*, 110–114. [[CrossRef](#)]
28. Barrera, D.; Madrigal, J.; Sales, S. Long Period Gratings in Multicore Optical Fibers for Directional Curvature Sensor Implementation. *J. Light. Technol.* **2018**, *36*, 1063–1068. [[CrossRef](#)]
29. Xu, S.; Chen, H.; Feng, W. Fiber-Optic Curvature and Temperature Sensor Based on the Lateral-Offset Spliced SMF-FCF-SMF Interference Structure. *Opt. Laser Technol.* **2021**, *141*, 107174. [[CrossRef](#)]
30. Yuan, W.; Zhao, Q.; Li, L.; Wang, Y.; Yu, C. Simultaneous Measurement of Temperature and Curvature Using Ring-Core Fiber-Based Mach-Zehnder Interferometer. *Opt. Express* **2021**, *29*, 17915. [[CrossRef](#)]
31. Liu, H.; Yang, H.; Qiao, X.; Wang, Y.; Liu, X.; Lee, Y.-S.; Lim, K.-S.; Ahmad, H. Curvature and Temperature Measurement Based on a Few-Mode PCF Formed M-Z-I and an Embedded FBG. *Sensors* **2017**, *17*, 1725. [[CrossRef](#)] [[PubMed](#)]

Disclaimer/Publisher’s Note: The statements, opinions and data contained in all publications are solely those of the individual author(s) and contributor(s) and not of MDPI and/or the editor(s). MDPI and/or the editor(s) disclaim responsibility for any injury to people or property resulting from any ideas, methods, instructions or products referred to in the content.